Electronic Supplementary Material (ESI) for Journal of Materials Chemistry A.


# Supporting Information

## A yolk@shell superhydrophobic/superhydrophilic solar evaporator for efficient and stable desalination

*Tao Hu*,[a] *Lingxiao Li*,[a] *Yanfei Yang*,[a] *Junping Zhang**,[a,b]

[a]Center of Eco-Material and Green Chemistry, Lanzhou Institute of Chemical Physics, Chinese Academy of Sciences, 730000 Lanzhou, P.R. China

[b]Center of Materials Science and Optoelectronics Engineering, University of Chinese Academy of Sciences, Beijing 100049, P.R. China

**E-mail address:* jpzhang@licp.cas.cn

**Supporting Discussion: Calculation of heat losses**

The heat loss of the solar evaporation device contains three parts: (a) radiation, (b) convection, (c) conduction.

a) Radiation: The radiation loss is calculated by the Stefan-Boltzmann equation.[1]

$$Q_{rad} = \varepsilon A\sigma(T_1^4-T_2^4) \quad (1)$$

Where $Q_{rad}$ represents heat flux, ε is the emissivity, A denotes the surface area, σ is the Stefan-Boltzmann constant ($5.67 \times 10^{-8}$ W $m^{-2}$ $K^{-4}$), $T_1$ (318.15 K) is the average surface temperature of the evaporator for a steady state of ~1 h, and $T_2$ (310.15 K) is the ambient temperature upward the evaporator under 1 sun irradiation. According to the equation, the radiation heat loss is ~5 %.

b) Convection: The convective heat loss is defined by the Newton' law of cooling.[2]

$$Q_{conv} = hA(T_1-T_2) \quad (2)$$

Where $Q_{conv}$ denotes the heat energy, h is the convection heat transfer coefficient, which is ~5 W $m^{-2}$ K. ΔT is the difference between the average surface temperature and the ambient temperature upward the evaporator (ΔT = 8 K). According to the equation, the convection heat loss is ~4%.

c) Conduction: The conduction loss was calculated based on.[3]

$$Q_{cond} = Cm\Delta T \quad (3)$$

Where $Q_{cond}$ is the heat energy, C is the specific heat capacity of water (4.2 J $K^{-1}$ $g^{-1}$), m (80 g) is the water weight, and ΔT (0.6 K) is the temperature difference of pure water after and before solar illumination under 1 sun for 1 h. Therefore, the

conduction heat loss is ~3%.

The phenomenon of high efficiency and relatively high heat loss is explained below.

(i) In the continuous irradiation process, the surface temperature of the evaporator, the temperature of the bulk water and the temperature around the environment are constantly changing. The fixed value taken in the calculation makes the calculation result in error.

(ii) The error induced by the infrared temperature measurement.

(iii) The surface of the evaporator is very rough. Thus, the surface area of the evaporator is larger than the projected area for the calculation of the efficiency and heat losses.

**Table S1.** Effect of MWCNTs concentration on evaporation rate.

| MWCNTs concentration (mg $mL^{-1}$) | 0.125 | 0.25 | 0.5 | 1 | 2 |
|---|---|---|---|---|---|
| Evaporation rate (kg $m^{-2}$ $h^{-1}$) | 0.95±0.2 | 1.23±0.3 | 1.45±0.3 | 1.44±0.4 | 1.45±0.2 |

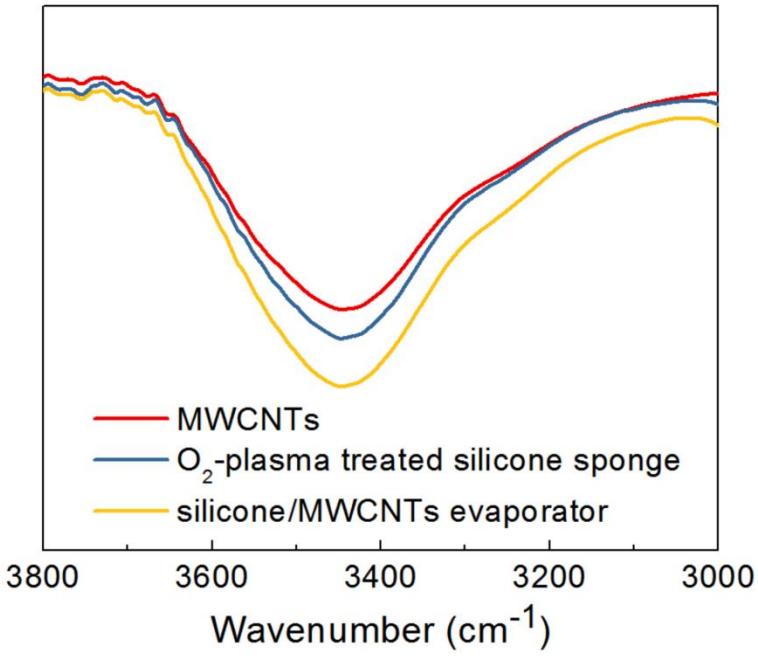


**Fig. S1** FTIR spectra of acid activated MWCNTs, $O_2$-plasma treated silicone sponge and the silicone/MWCNTs evaporator. The bands at 3300~3500 $cm^{-1}$ are attributed to stretching vibrations of hydroxyl groups. Compared to the bands of MWCNTs and $O_2$-plasma treated silicone sponge, the band of the silicone/MWCNTs evaporator is widened and enhanced. This means hydrogen bonding between MWCNTs and silicone sponge, which increased polarization degree of the O-H bond.[4]

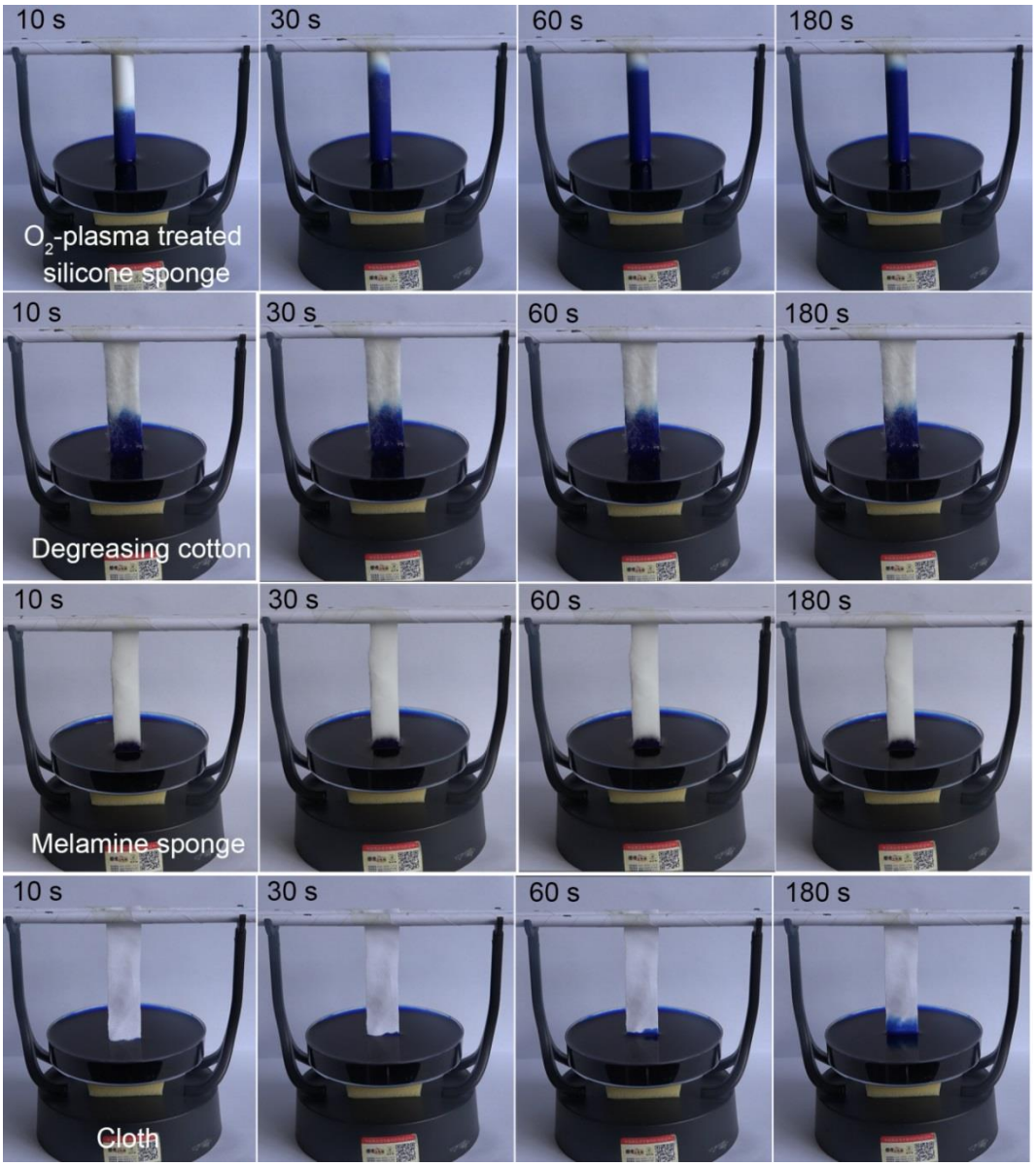


**Fig. S2** Climbing behaviors of water dyed with methylene blue in the shell of the $O_2$-plasma treated silicone sponge and some other conventional matrices for water transport during solar evaporation.

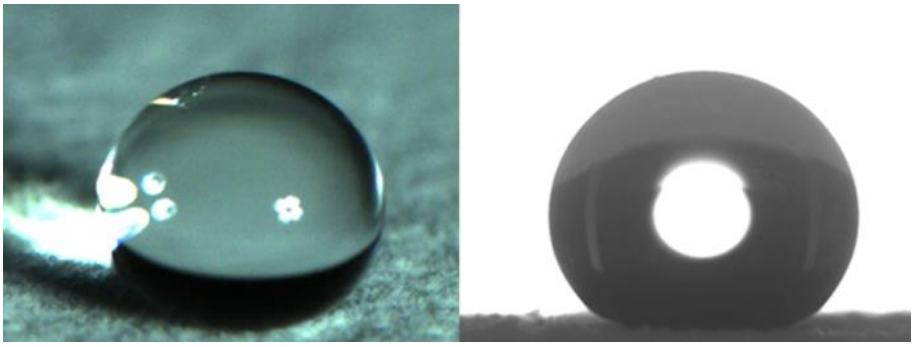

**Fig. S3** Photographs of water droplets on the superhydrophobic yolk of the silicone/MWCNTs evaporator.

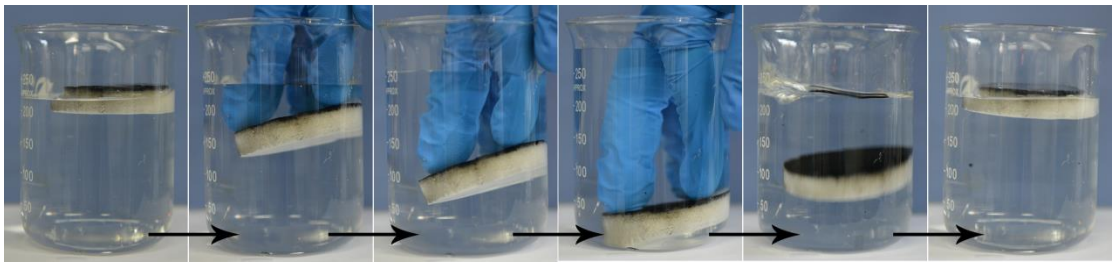

**Fig. S4** Representative photographs of the silicone/MWCNTs evaporator in 20 cycles of squeezing and releasing in water.

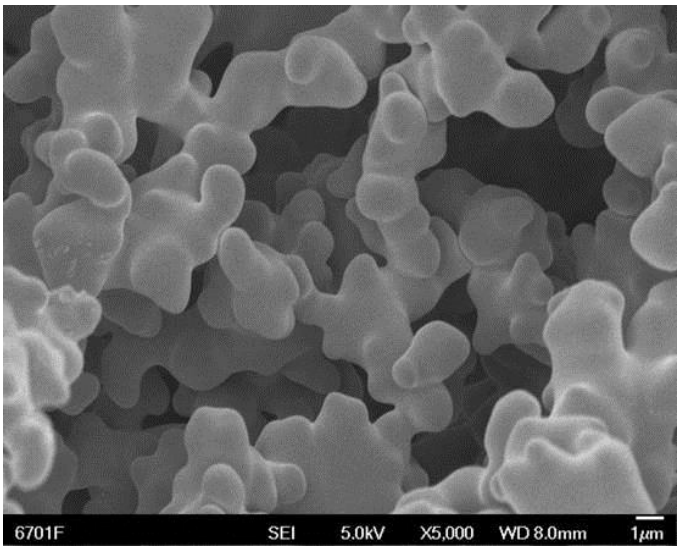


**Fig. S5** Cross-sectional SEM image of the silicone/MWCNTs evaporator after 100 compression-release cycles with 50% strain.

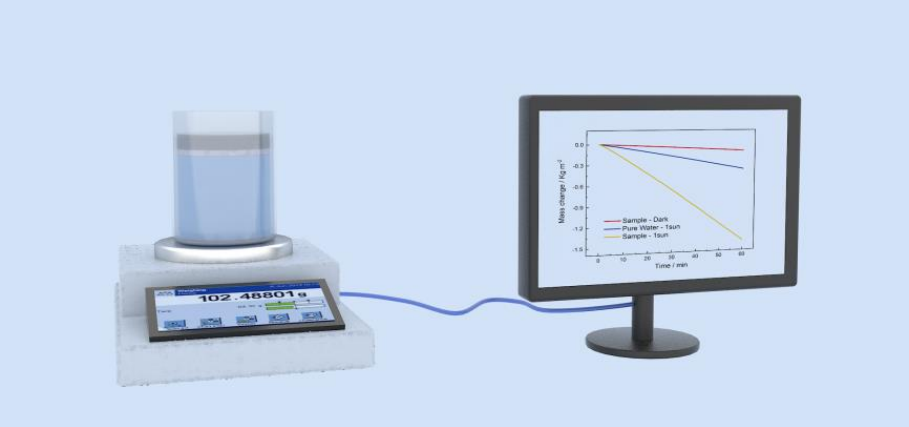


**Fig. S6** Photograph of the custom made setup for testing the solar evaporation properties of the silicone/MWCNTs evaporators.

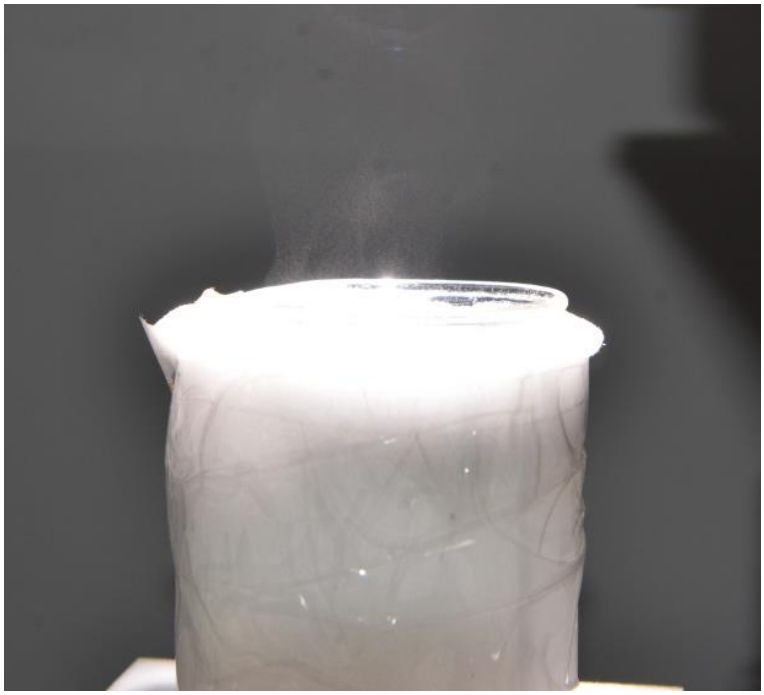

**Fig. S7** Photograph of water vapor generated by the silicone/MWCNTs evaporator under 2 sun.

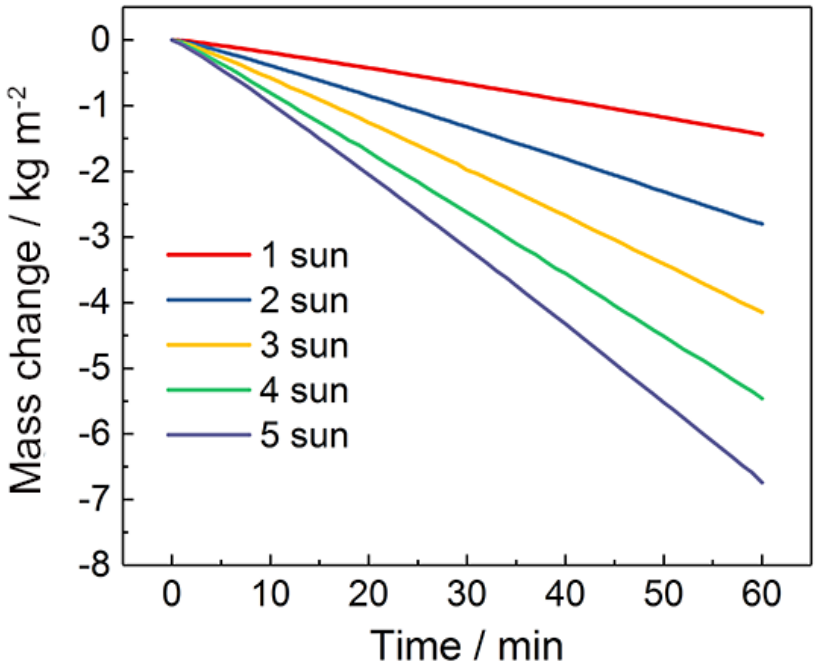


**Fig. S8** Water mass changes versus time under different illuminations in the presence of the silicone/MWCNTs evaporator.

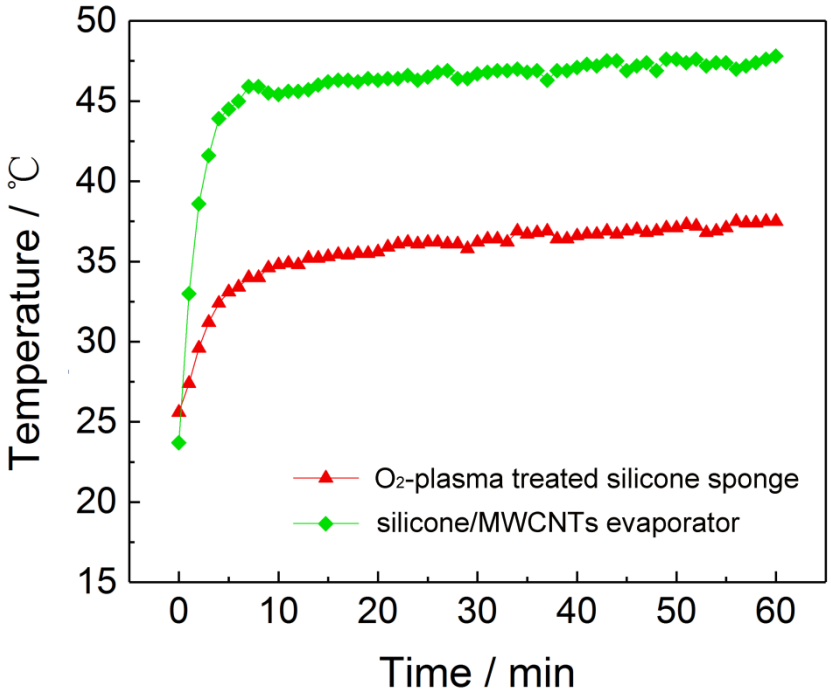


**Fig. S9** Variation of top surface temperature of the silicone/MWCNTs evaporator under 1 sun with the $O_2$-plasma treated silicone sponge for comparison.

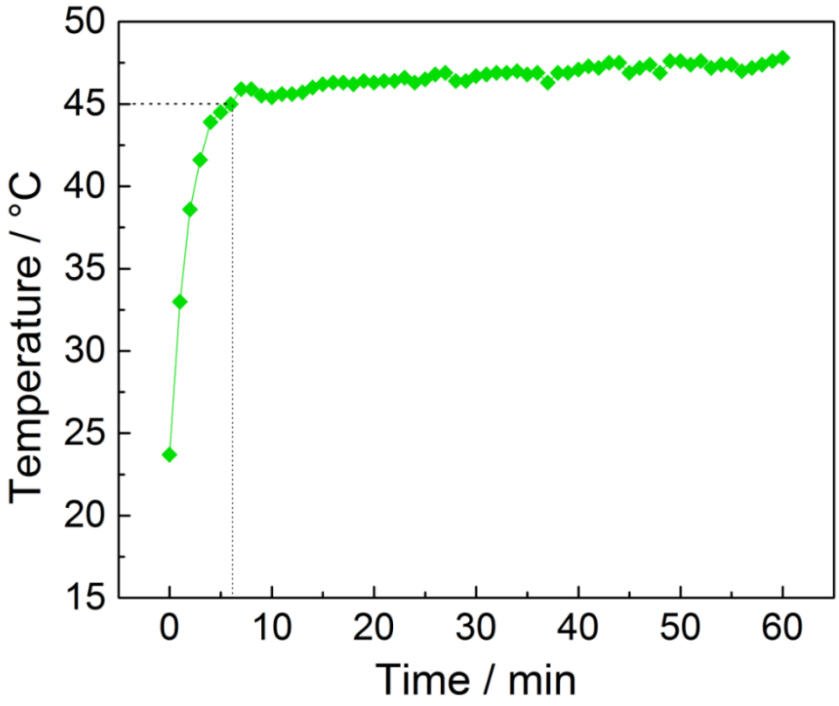


**Fig. S10** Variation of top surface temperature of the silicone/MWCNTs evaporator with irradiation time under 1 sun.

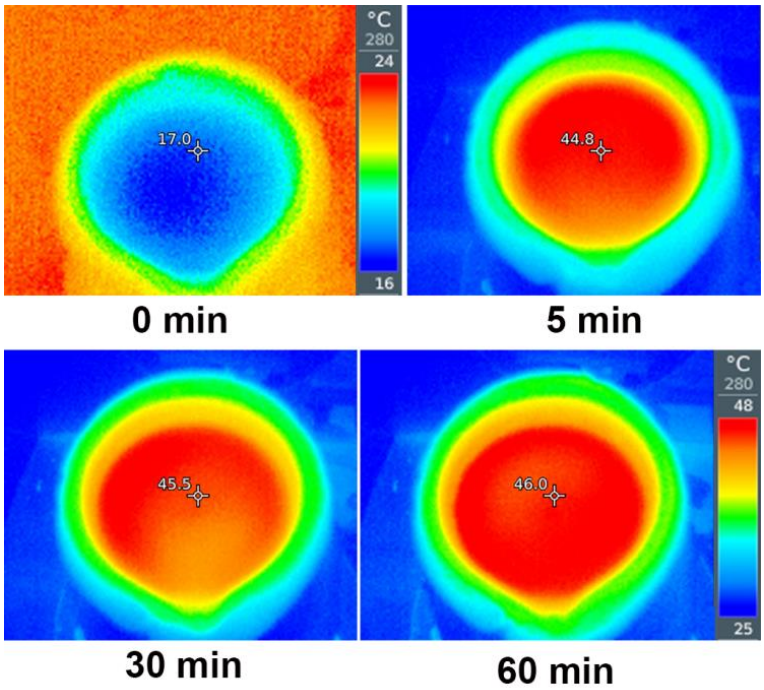


**Fig. S11** Infrared images of top surface of the silicone/MWCNTs evaporator under 1 sun.

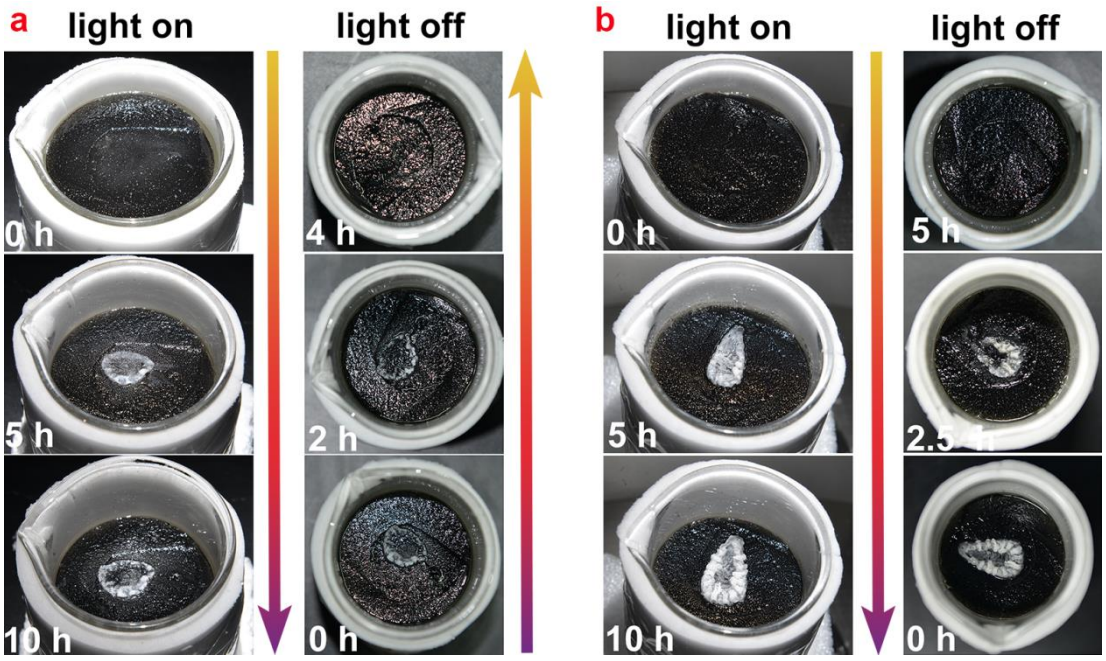


**Fig. S12** Salt precipitation (1 sun) and salt ablation (room conditions) processes of seawater from (a) the Bohai Sea and (b) the Yellow Sea on the top surface of the silicone/MWCNTs evaporator.

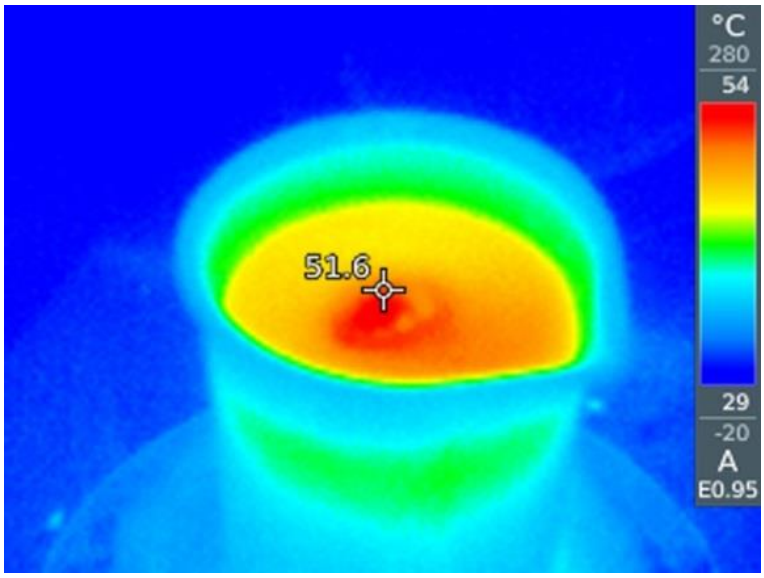


**Fig. 13** Infrared image of the evaporator surface after continuous irradiation for 2 h under 1 sun.

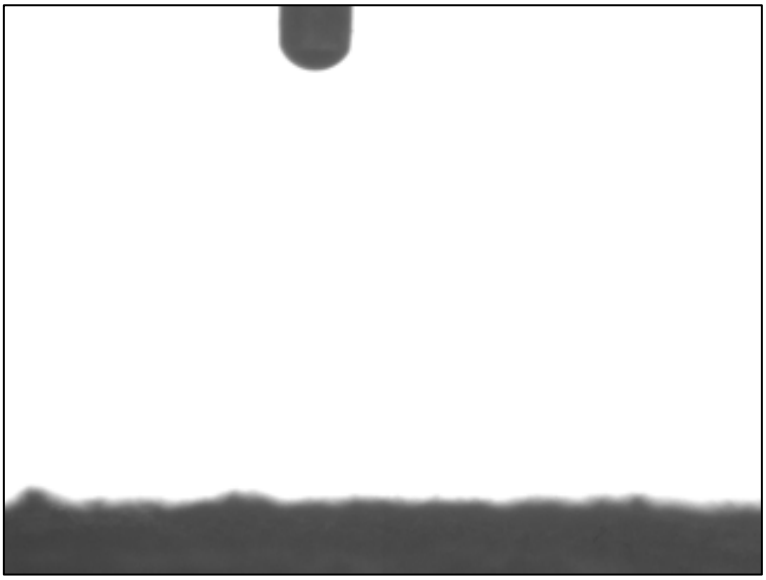

**Fig. 14** Measurement of water CA of the shell of the silicone/MWCNTs evaporator after being soaked in 3.5 wt% NaCl solution for 30 d.

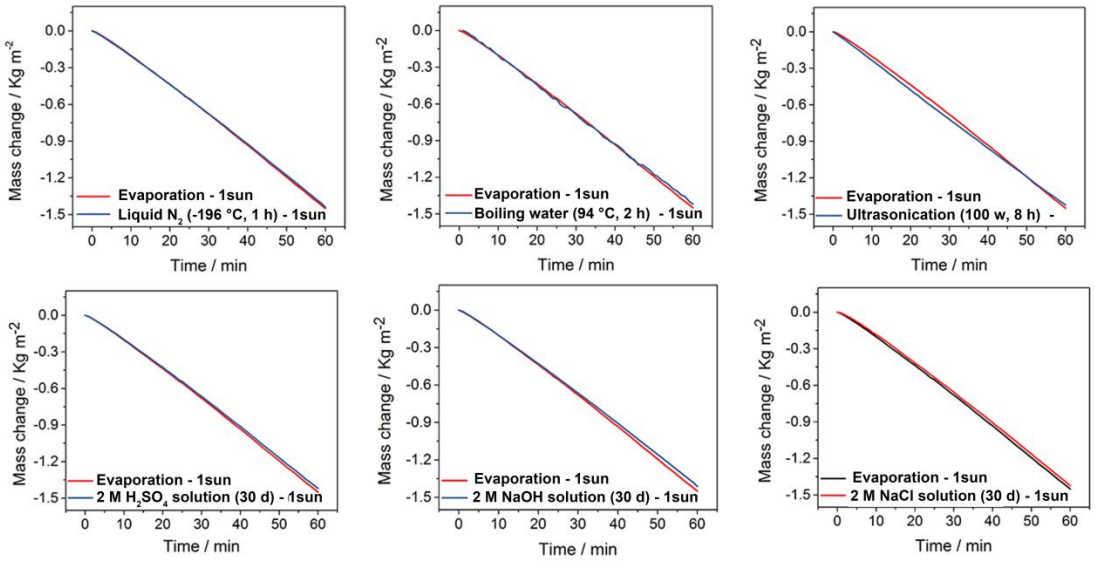


**Fig. S15** Water mass changes of the silicone/MWCNTs evaporator after immersion in liquid $N_2$ (-196 °C, 1 h), boiling water (94 °C, 2 h), deionized water under ultrasonication (100 w, 8 h), 2 M $H_2SO_4$ solution (30 d), 2 M NaOH solution (30 d) and 2 M NaCl solution (30 d).

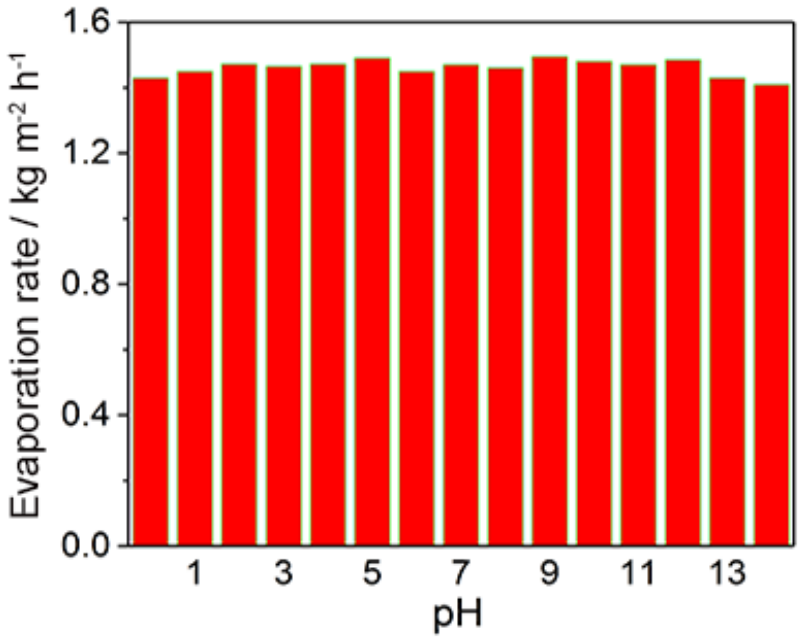


**Fig. S16** Evaporation rate of aqueous solutions with different pH under 1 sun illumination. The pH of the aqueous solutions was regulated using 1 M $H_2SO_4$ solution and 1 M NaOH solution.

**Movie S1.** Impacting of a 10 μL water droplet from a height of 10 mm on the shell of the evaporator. This video highlights the superhydrophilicity of the shell and ultrafast water transport in the shell.

**Movie S2.** Climbing behaviors of water dyed with methylene blue in the shell of the $O_2$-plasma treated silicone sponge and some other conventional matrices for water transport during solar evaporation. This video highlights the much faster water transport in the shell of the $O_2$-plasma treated silicone sponge than the others.

**Movie S3.** Impacting of a 10 μL water droplet from a height of 10 mm on the yolk of the evaporator. This video highlights the superhydrophobicity of the yolk.

**References**


1. G. Ni, G. Li, Svetlana V. Boriskina, H. Li, W. Yang, T. Zhang and G. Chen, *Nat. Energy*, 2016, **1**, 16126.

2. K. Yin, S. Yang, J. Wu, Y. Li, D. Chu, J. He and J.-A. Duan, *J. Mater. Chem. A,* 2019, **7**, 8361-8367.

3. X. Li, W. Xu, M. Tang, L. Zhou, B. Zhu, S. Zhu and J. Zhu, *Proc. Natl. Acad. Sci.U.S.A.*, 2016, **113**, 13953-13958.

4. T. Fornaro, D. Burini, M. Biczysko, and V. Barone, *J. Phys. Chem. A* 2015, **119**, 4224-4236.